Chemical Modeling of the Oxygen-Evolving Center in Plants. Synthesis, Structure, and Electronic and Redox Properties of a New Mixed Valence Mn−Oxo Cluster: $[Mn_2^{III,IV}O_2(bisimMe_2en)_2]^{3+}$ ($bisimMe_2en$ = *N*,*N*′-Dimethyl-*N*,*N*′-bis(imidazol-4-ylmethyl)ethane-1,2-diamine). EPR Detection of an Imidazole Radical Induced by UV Irradiation at Low Temperature

Yves-Michel Frapart,[1a] Alain Boussac,*[,1b] Rolf Albach,[1a] Elodie Anxolabéhère-Mallart,[1a] Michel Delroisse,[1c] Jean-Baptiste Verlhac,[1c] Geneviève Blondin,[1a] Jean-Jacques Girerd,*[,1a] Jean Guilhem,[1d] Michèle Cesario,[1d] Alfred William Rutherford,[1b] and Doris Lexa[1e]

Contribution from the Laboratoire de Chimie Inorganique, URA CNRS 420, Institut de Chimie Moléculaire d'Orsay, Université Paris-Sud, 91405 Orsay, France, Département de Biologie Cellulaire et Moléculaire, SBE, URA CNRS 1290, CEA Saclay, 91 191 Gif-sur-Yvette, France, Laboratoire de Chimie Organique et Organométallique, URA CNRS 35, Université de Bordeaux, 33 405 Talence Cedex, France, Institut de Chimie des Substances Naturelles, UPR CNRS 2301, 91198 Gif-sur-Yvette, France, and Laboratoire de Bioénergétique et Ingéniérie des Protéines, UPR CNRS 9036, 13 009 Marseille, France

Received November 8, 1994. Revised Manuscript Received November 26, 1995[⊗]

Abstract: The compound $[Mn_2^{III,IV}O_2(bisimMe_2en)_2](ClO_4)_3\cdot H_2O$ ($bisimMe_2en$ = *N*,*N*′-dimethyl-*N*,*N*′-bis(imidazol-4-ylmethyl)ethane-1,2-diamine) was synthesized. It crystallizes in the monoclinic space group *C*2/*c* with $a = 18.139(8)$ Å, $b = 12.694(5)$ Å, $c = 17.694(8)$ Å, $\beta = 107.5(6)°$, $V = 3885(6)$ Å^3, and $Z = 4$. The cation $[Mn_2^{III,IV}O_2(bisimMe_2en)_2]^{3+}$ contains a di-manganese di-μ-oxo unit. The Mn−Mn axis is a C_2 axis. The Mn−imidazole distances for Mn^{III} or Mn^{IV} are distinct: respectively, 2.208(9) and 2.004(8) Å. The ground state is a $|S_A{=}2,S_B{=}^3/_2,S{=}^1/_2\rangle$ state separated by 420 cm^{-1} from the $S = {}^3/_2$ state. The EPR spectrum has been simulated with $|A_{1x,y}| = 160.10^{-4}$ cm^{-1}, $|A_{1z}| = 136.10^{-4}$ cm^{-1}, $|A_{2x,y}| = 72.10^{-4}$ cm^{-1}, $|A_{2z}| = 71.10^{-4}$ cm^{-1}, $g_{xy} = 1.997$, $g_z = 1.993$. The ESEEM spectrum is reported. The ^{2}H nuclei corresponding to the exchangeable hydrogen atoms of imidazole groups in D_2O have been detected at 2.4 MHz at 3480 G. In cyclic voltammetry, $[Mn_2^{III,IV}O_2(bisimMe_2en)_2]^{3+}$ presents in oxidation two reversible waves at 1.04 and 1.40 V (all potentials versus NHE) in strong contrast with what has been always observed on other $Mn_2^{III,IV}O_2$ units, for which only one wave in oxidation ([III,IV] → [IV,IV]) is observed. EPR spectroelectrochemistry reveals the disappearance of the 16 line spectrum of the [III,IV] species on oxidation at 1.24 V. UV-vis spectroelectrochemistry at this potential confirms the formation of the [IV,IV] dimer. The existence of two waves was related to the presence of slow equilibrium between two different [III,IV] forms. UV-irradiation of the starting $[Mn_2^{III,IV}O_2(bisimMe_2en)_2]^{3+}$ complex in an aqueous borate buffer at pH = 10 at 77 K resulted in the formation of an EPR signal that is attributed to an imidazole radical coupled to the $Mn^{III}-Mn^{IV}$ pair. This signal is unsplit and is understandable in a simple model of two spins $S = {}^1/_2$ in magnetic interaction. It has some analogy with that observed by Boussac et al. (*Nature* **1990**, *347*, 303−306) on the S_3 state of the Ca^{2+} and Cl^--depleted oxygen-evolving center, although in that case the signal was split. We relate this difference to small differences in the magnetic interaction of the two spins $S = {}^1/_2$. ESEEM spectra of the irradiated $[Mn_2^{III,IV}O_2(bisimMe_2en)_2]^{3+}$ complex are reported for magnetic fields corresponding to the resonance of the radical or the metal cluster. These results suggest that the formed imidazole radical stays linked to the metal core despite the weak magnetic interaction detected. This rises the possibility that the S_3 radical in the natural system, is a direct ligand to Mn cluster.

Introduction

A cluster of four Mn located in the reaction centre of PS-II probably acts both as the active site and as a charge accumulating device of the water-splitting enzyme in photosystem II.[2] During the enzyme cycle, the oxidizing side of PS-II goes through five different redox states that are denoted S_n, *n* varying from 0 to 4.[3] The oxygen is released during the S_3 to S_0 transition in which S_4 is a transient state. The S_2 state is characterized by a multiline EPR signal[4] which arises from the

[⊗] Abstract published in *Advance ACS Abstracts,* February 15, 1996.

(1) (a) Université Paris-Sud. (b) CEA Saclay. (c) Université de Bordeaux. (d) Institut de Chimie des Substances Naturelles. (e) Marseille.

(2) For reviews, see Debus, R. J. *Biochem. Biophys. Acta* **1992**, *1102*, 269−352 and Rutherford, A. W. *Trends Biochem. Sci.* **1989**, *14*, 227−232.

(3) Kok, B.; Forbush, B.; McGloin, M. *Photochem. Photobiol.* **1970**, *11*, 457−475.

(4) Dismukes, C. G.; Siderer, Y. *Proc. Natl. Acad. Sci. U.S.A.* **1981**, *78*, 274−278.

0002-7863/96/1518-2669$12.00/0

magnetic interaction between the four Mn resulting in a spin $^1/_2$ system.[5]

The ligands to the Mn cluster have not yet been identified.[2] ESEEM experiments done on the S_2 Mn multiline signal showed ^{14}N coupling and were taken as an indication of one or more imidazole ligands.[6] In a recent study using histidine specifically ^{15}N labeled on the imidazole ring, the coupling of the Mn to imidazole nitrogens was unequivocally demonstrated.[7]

Ca^{2+} and Cl^- are two essential cofactors for oxygen evolution.[2,8−10] In Ca^{2+}- and Cl^--depleted PS-II, inhibition of the enzyme cycle occurs at the S_3 to S_0 transition.[2,9,11] Formation of the S_3-state in Ca^{2+}-depleted and Cl^--depleted PS-II results in the appearance of a split EPR signal centered at $g = 2$ with a line width of 130 to 164 gauss. The appearance of the split S_3 EPR signal is accompanied by the disappearance of the S_2 multiline signal in cw-EPR.[12,13] The S_3 signal was originally interpreted as an organic free radical interacting magnetically with the Mn cluster.[12,13] From its UV visible spectrum, the radical was suggested to be a histidine radical.[13] However, this radical has not been unambiguously assigned. Recent ENDOR evidence has been taken as an indication that a tyrosine radical is involved.[14] As yet no studies have been reported of appropriate model systems of imidazole or phenol radicals interacting with Mn clusters.

The assignment of the S_3 state to an oxidized radical led to the proposal that the Mn cluster itself remained in the same redox state as in the S_2 state, although it became undetectable as an EPR multiline signal. This was backed up by EPR simulations demonstrating that a simple weak magnetic interaction required for generating the split EPR signal could also explain the disappearance of the hyperfine lines from the Mn signal.[13] Subsequently, experimental support for this model was obtained when a broad electron spin echo spectrum attributed to the Mn signal lacking the hyperfine lines was detected in the presence of S_3 radical.[15]

There has been some debate about the proximity of the radical to the Mn cluster. The simulation of the magnetic interaction between the radical and the cluster used distance parameters which placed the radical outside the first coordination sphere of the Mn.[13] However, the lack of spectral features in the organic radical spectrum due to overlap with the stable tyrosine radical makes this simulation somewhat oversimplified. The possibility that the radical could be on a residue which ligands to the Mn cluster remains open.

In summary, recent spectroscopic studies of the water-splitting enzyme have indicated not only that the Mn cluster has imidazole ligation but also that a histidine or a tyrosine close to Mn, possibly a ligand, can undergo oxidation. Thus investigations of synthetic Mn clusters liganded with imidazole are warranted. Collins et al. in 1987[16] reported the synthesis of a $Mn^{III}-Mn^{IV}$ complex using the ligand bispicen. Variations of this type of ligand have been studied.[17] We here report a modification where the pyridine groups are replaced by imidazoles and the nitrogen atoms of the ethylenediamine link are methylated. The $Mn^{III}-Mn^{IV}$ complex is described. This allows the study of the interaction between imidazole groups and a Mn cluster. Moreover, an organic radical, attributed to imidazole, was generated in the complex by UV irradiation.

Experimental Section

Compound Preparation. All chemical syntheses were performed under aerobic conditions using Aldrich starting materials as received. Solvents were dried before use. NMR spectra were recorded on a Bruker AC250 spectrometer.

Caution! Perchlorate salts of metal complexes with organic ligands are potentially explosive. Only small quantities of these compounds should be prepared and handled behind suitable protective shields.

For electrochemical experiments, tetrabutylammonium perchlorate (TBAP, Fluka, puriss) was used as supporting electrolyte. Acetonitrile (Merck, uvasol) was used without further purification.

***N,N′*-Dimethyl-*N,N′*-bis(imidazol-4-ylmethyl)ethane-1,2-diamine ((bisimMe_2en)·4HCl).** 4-(Chloromethyl)imidazole hydrochloride was prepared in 75% yield from 4-(hydroxymethyl)imidazole by treatment with thionyl chloride in toluene.[18] It was then added portionwise (4.6 g, 40 mmol) to a solution of *N,N′*-dimethyl-1,2-diaminoethane (1.7 g, 20 mmol) and triethylamine (11.1 mL, 80 mmol) in absolute ethanol (30 mL). The suspension was refluxed for 2 h and evaporated in vacuum. A saturated aqueous sodium carbonate solution was added to the gummy product, and the solution was evaporated to dryness. Inorganic salts were precipitated by dissolving the residue in a chloroform/ethanol mixture. The ligand was isolated as the tetrahydrochloride salt by bubbling HCl gas in an ethanol solution. Recrystallization in methanol afforded 4.4 g (57 %) of a pale yellow solid. Mp 208−210 °C. ^{1}H NMR (250 MHz, D_2O) δ 2.86 (s, 6H), 3.73 (s, 4H), 4.6 (s, 4H), 4.82 (bs, 6H), 7.78 (s, 2H), 8.78 (s, 2H). ^{13}C NMR (62.9 MHz, D_2O) d 40.86, 50.58, 50.68, 124.03, 125.16, 137.02. Anal. Calcd for $C_{12}H_{24}N_6Cl_4 \cdot {}^1/_2H_2O$: C, 35.75; H, 6.25; N, 20.84. Found: C, 35.51; H, 6.48; N, 20.25.

$[Mn_2O_2$(bisimMe_2en)$_2](ClO_4)_3 \cdot H_2O$. This complex was prepared according to the method described by Hodgson et al.[19] Sodium hydrogenocarbonate was added to a mixture of bisimMe_2en·4HCl (0.79 g, 2 mmol) and $MnCl_2 \cdot 4H_2O$ (0.4 g, 2 mmol) in water (10 mL) until the pH of the solution reached neutrality (careful control of the pH, which must be within 6.5 and 7, is very important). A few drops of a 33% aqueous hydrogen peroxide solution were added to the mixture which became deep green-brown. Addition of sodium perchlorate (2 g) allowed precipitation of the complex, which was recrystallized from water. Yield 38%. Anal. Calcd for $C_{24}H_{40}Cl_3Mn_2N_{12}O_{14} \cdot H_2O$: C, 30.19; H, 4.43; N, 17.60; Cl, 11.14; Mn, 11.51. Found: C, 30.70; H, 4.81; N, 17.43; Cl; 11.05; Mn, 11.45. Crystals were obtained by vapor diffusion of a dichloroethane−chloroform (1/1) mixture into an acetonitrile solution of the complex. After a few days, dark crystals were collected.

Cyclic Voltammetry. Cyclic voltammetry was measured using an homemade potentiostat and a current measurer equipped with a positive feedback ohmic drop compensation, a Parr (175) function generator, and a X-Y chart recorder (IFELEC 2502). As the working electrode, glassy carbon (Tokai, Japan: $\Phi = 3$ mm) provided the best results. It was carefully polished with diamond pastes and ultrasonically rinsed in ethanol before each potential run. An Au wire was used as auxiliary

(5) Bonvoisin, J.; Blondin, G.; Girerd, J.-J.; Zimmermann, J.-L. *Biophys. J.* **1992**, *61*, 1076−1086.
(6) Britt, R. D.; Zimmermann, J.-L.; Sauer, K.; Klein, M. P. *J. Am. Chem. Soc.* **1989**, *111*, 3522−3532.
(7) Tang, X.-S.; Diner, B. A.; Larsen, B. S.; Gilchrist, M. L., Jr.; Lorigan, G. A.; Britt, R. D. *Proc. Natl. Acad. Sci. U.S.A.* **1994**, *91*, 704−708.
(8) Homann, P. H. *J. Bioenerg. Biomembr.* **1987**, *19*, 105−123.
(9) Rutherford, A. W.; Zimmermann, J.-L.; Boussac, A. In *The Photosystems: Structure, Function and Molecular Biology*; Barber, J., Ed.; Elsevier Science Publishers: New York, 1992; Chapter 5, pp 179−229.
(10) Yocum, C. F. *Biochim. Biophys. Acta* **1991**, *1059*, 1−15.
(11) Boussac, A.; Rutherford, A. W. *Biochem. Soc. Trans.* **1994**, *22*, 352−358.
(12) Boussac, A.; Zimmermann, J.-L.; Rutherford, A. W. *Biochemistry* **1989**, *28*, 8984−8989.
(13) Boussac, A.; Zimmermann, J.-L.; Rutherford, A. W.; Lavergne, J. *Nature* **1990**, *347*, 303−306.
(14) Gilchrist, M. L.; Ball, J. A.; Randall, D. W.; Britt, R. D. *Proc. Natl. Acad. Sci. U.S.A.* **1995**, *92*, 9545−9549.
(15) Zimmerman, J.-L.; Boussac, A.; Rutherford, A. W. *Biochemistry* **1993**, *32*, 4831−4841.
(16) Collins, M.; Hodgson, D. J.; Michelsen, K.; Towle, D. K. *J. Chem. Soc., Chem. Commun.* **1987**, 1659−1660.
(17) Goodson, P. C.; Glerup, J.; Hodgson, D. J.; Michelsen, K.; Weihe, H. *Inorg. Chem.* **1991**, *30*, 4909−4914.
(18) Turner, R. A.; Huebner, C. F.; Scholtz, C. R. *J. Am. Chem. Soc.* **1949**, *71*, 2801. Kaptein, B.; Barf, R.; Kellog, R. M.; Van Bolhuis, F. *J. Org. Chem.* **1990**, *55*, 1890.
(19) Goodson, P. C.; Oki, A. R.; Glerup, J.; Hodgson, D. J. *J. Am. Chem. Soc.* **1990**, *112*, 6248.

Table 1. Crystallographic Data for $[Mn_2O_2(bisimMe_2en)_2](ClO_4)_3 \cdot H_2O$

formula	$C_{24}H_{40}Cl_3Mn_2N_{12}O_{14} \cdot H_2O$
fw	954.919
radiation	Mo Kα (0.7107 Å)
temp, K	294
space group	*C*2/*c*
a, Å	18.139(8)
b, Å	12.694(5)
c, Å	17.694(8)
α, deg	90.0
β, deg	107.5(6)
γ, deg	90.0
V, Å^3	3885(6)
Z	4
μ, mm^{-1}	0.9
N_{meas}	4102
$N_{obs}[3\sigma(I)]$	1743
R	0.055
R_w	0.061

electrode and a $Ag/AgClO_4$ electrode prepared in acetonitrile, separated by a fritted disk from the main solution as reference (400 mV above the potential of the saturated calomel electrode). The experiments were carried out in a double-wall Pyrex cell (thermostated with 2-propanol) protected from light, on carefully degassed solutions by argon flushing. All potentials in this paper are indicated versus NHE.

Preparative Scale Electrolysis. They were carried out on a large glassy carbon electrode with the same reference electrode and a larger auxiliary electrode separated from the bulk solution by a large fritted disk. The charges were measured with a Tacussel IGN 5 integrator, and the intensity with an amperemeter Peckly Didact A430. The potential was imposed with a Tacussel PRT100-1X potentiostat and controlled with a Keithley 175A multimeter.

EPR Spectroelectrochemistry. The thin layer cell used for room temperature EPR experiments was previously described.[20] The working electrode consisted of a platinum grid.

UV-vis Spectroelectrochemistry. The thin layer cell used for room temperature UV-vis experiments was previously described.[21] Due to the sensitivity to light of the most oxidized species, we used a diode array HP8452 spectrophotometer. The working electrode consisted of a platinum grid.

Magnetic Susceptibility Measurements. Magnetic susceptibility measurements in the 4.2−300 K temperature range were carried out with a Faraday-type magnetometer equipped with a helium continuous-flow cryostat. The automatic data-acquisition equipment was made at the Laboratoire de Chimie Inorganique. $HgCo(NCS)_4$ was used as a susceptibility standard.

Crystallographic Data Collection and Refinement of the Structure. A single crystal of dimensions 0.3 × 0.4 × 0.8 mm was mounted on a four-circle Philips diffractometer with graphite monochromated Mo Kα radiation ($\lambda = 0.7107$ Å). The data collection was with $\theta-2\theta$ scan technique mode (range 2−28°, speed 0.200° s^{-1}, scan width 1.2°). Three standard reflections were measured every 180 min and showed no decay. A total of 4102 reflections [$-23 < h < 23$, $0 < k < 16$, $0 < l < 23$] was collected. From 3688 unique reflections, 1748 were considered as observed [$I > 3\sigma(I)$]. Lorentz polarization and empirical absorption corrections[22] were applied.

The crystallographic data are collected in Table 1. The unit cell contains 4 cations $[Mn_2^{III,IV}O_2(bisimMe_2en)_2]^{3+}$ with a di-manganese di-μ-oxo unit, 12 perchlorate anions, and 4 water molecules. The Mn^{III} and Mn^{IV} atoms are located on the C_2 axis; the asymmetric unit consists of half a unit. The structure was solved by direct methods (Program SHELXS86),[23] and refined by full-matrix least squares, minimizing the function $\sum w(|F_o| - |F_c|)^2$ (Program SHELX76).[24] Anisotropic thermal parameter refinement was performed except for oxygen atoms of ClO_4^- ions.

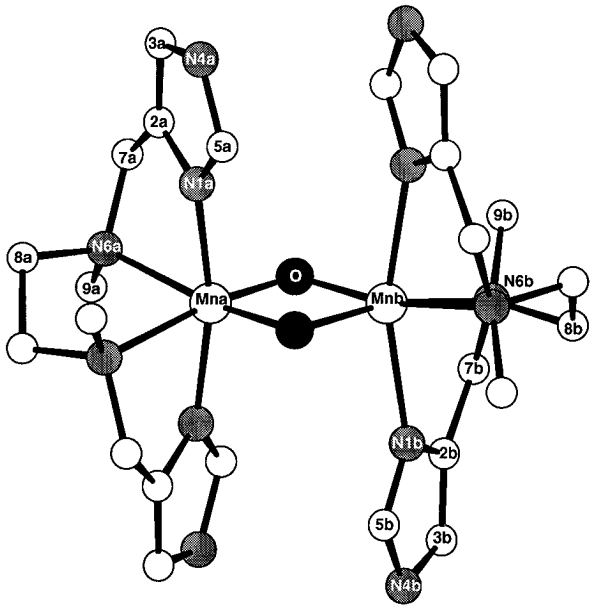

Figure 1. Structure of $[Mn_2O_2(bisimMe_2en)_2]^{3+}$ showing the atom-labeling scheme. Hydrogen atoms are omitted.

Perchlorate anions are located in general positions, with partial occupancy for one of the two counterions (occupancy factor 1.0 for anion labeled Cl11 and 0.5 for Cl21). Moreover, strong disorder was observed for oxygen atoms around the chlorine pivot atoms. Five positions have been located on difference Fourier maps for the perchlorate anion Cl11 and two for the Cl21 anion. Refinement with constraints[25] to the Cl−O atom distances was performed. All hydrogen atoms of the cationic unit were located on difference synthesis and included in the refinement with isotropic thermal parameters. Final weighting scheme was $w = [\sigma^2(F) + 0.004F^2]^{-1}$, σ from counting statistics. The final conventional *R* factors are $R = 0.055$ and $Rw = 0.061$ for 1743 reflections and 299 parameters.

EPR Spectra. EPR spectra were recorded on Bruker ER 200 D and 300 spectrometers at X-band. For low temperature studies, an Oxford Instruments continuous flow liquid helium cryostat and a temperature control system were used.

Pulsed EPR was done with a Bruker ESP 380 spectrometer already described.[15] The field-swept spectra were obtained by measuring the amplitude of the echo as a function of the magnetic field after a two-pulse sequence ($\pi/2-\tau-\pi$). The duration of $\pi/2$ and π pulses were 8 and 16 ns, respectively. The ESEEM data presented in this work result from a three-pulse sequence ($\pi/2-\tau-\pi/2-T-\pi/2$). In the 2D experiments, the minimum τ and *T* values were 120 and 24 ns, respectively. The *T* value was incremented by 8 ns steps and the τ value by 16 ns steps. The $\pi/2$ pulse duration was 16 ns. To remove the unwanted echoes in a three-pulse experiment, the phase cycling procedure described in ref 26 was used.

For the EPR experiments in which the samples were UV-irradiated, the complex was solubilized in distilled water containing 0.25 M borate and 0.25 M NaCl buffered at pH 10 with NaOH. Then the sample was immediately put into an EPR tube and frozen quickly to 77 K. UV irradiation was done at 77 K with a 1000 W Hg/Xe lamp (Oriel). The sample was UV-irradiated in the EPR tube which was immersed in a non-silvered quartz dewar filled with liquid nitrogen.

Results and Discussion

I. The $[Mn_2O_2(bisimMe_2en)_2]^{3+}$ Species. Structure. The structure of the $[Mn_2O_2(bisimMe_2en)_2]^{3+}$ cation is represented in Figure 1. It contains a dimanganese−di-μ-oxo unit in which

(20) Lexa, D.; Momenteau, M.; Mispelter, J.; Savéant, J.-M. *Inorg. Chem.* **1989**, *28*, 30−35.
(21) Lexa, D.; Savéant, J.-M.; Zickler, J. *J. Am. Chem. Soc.* **1977**, *99*, 2786.
(22) Walker, N.; Stuart, D. *Acta Crystallogr.* **1983**, *A39*, 158−166.
(23) Sheldrick, G. M. SHELX86, Program for Crystal Structure Solution; University of Göttingen; Göttingen, Germany, 1986.
(24) Sheldrick, G. M. SHELX76, Program for Crystal Structure Solution; University of Cambridge; Cambridge, England, 1976.
(25) Waser, J. *Acta Crystallogr.* **1963**, *16*, 1091−1094.
(26) Kevan, L. In *Modern Pulsed and Continuous Wave Electron Spin Resonance*; Kevan, L., Bowaman, M. K., Eds.; Wiley Interscience: New-York, 1990; pp 231−266.

Table 2. Bond Lengths (Å) and Angles (deg)

Mna−O	1.774(5)	Mnb−O	1.868(6)
Mna−N1a	2.004(8)	Mnb−N1b	2.208(9)
Mna−N6a	2.163(7)	Mnb−N6b	2.137(8)
Mna−Mnb	2.677(2)		
N1a−C2a	1.362(12)	N1b−C2b	1.385(14)
N1a−C5a	1.313(13)	N1b−C5b	1.321(14)
C2a−C3a	1.345(16)	C2b−C3b	1.344(17)
C2a−C7a	1.505(15)	C2b−C7b	1.512(16)
C3a−N4a	1.366(15)	C3b−N4b	1.361(16)
N4a−C5a	1.355(14)	N4b−C5b	1.367(16)
N6a−C7a	1.493(11)	N6b−C7b	1.503(15)
N6a−C8a	1.515(11)	N6b−C8b	1.529(14)
N6a−C9a	1.478(13)	N6b−C9b	1.502(16)
C8a−C8a′	1.522(12)		
O−Mna−N1a	97.2(3)	O−Mnb−N1b	99.7(3)
O−Mna−N6a	95.2(3)	O−Mnb−N6b	98.1(3)
O−Mna−O′	88.1(2)	O−Mnb−O′	82.6(2)
O−Mna−N1a′	91.5(3)	O−Mnb−N1b′	92.7(3)
O−Mna−N6a′	169.0(3)	O−Mnb−N6b′	168.4(3)
N1a−Mna−N6a	77.7(3)	N1b−Mnb−N6b	75.7(3)
N1a−Mna−N1a′	167.8(3)	N1b−Mnb−N1b′	163.5(3)
N1a−Mna−N6a′	93.1(3)	N1b−Mnb−N6b′	91.8(3)
N6a−Mna−N6a′	83.4(3)	N6b−Mnb−M6b′	83.4(3)
Mna−O−Mnb	94.6(3)		

the Mn−Mn axis is a C_2 axis. The inequivalence between the Mn^{IV} (Mn_a) and Mn^{III} (Mn_b) ions is quite recognizable from the bond distances (Table 2). The distances Mn_a-O and Mn_b-O are, respectively, equal to 1.774(5) and 1.868(6) Å. The Mn−imidazole distances Mn_a-N_{1a} and Mn_b-N_{1b} are, respectively, equal to 2.004(8) and 2.208(9) Å. The Mn−amine distances Mn_a-N_{6a} and Mn_b-N_{6b} are much less sensitive to the oxidation state of manganese: they are 2.163(7) and 2.137(8) Å, respectively. This is in agreement with a $d_\pi^3 d_z^{2\,1}$ configuration for Mn^{III} (the *z* axis is perpendicular to the Mn_2O_2 plane). The d_z^2 orbital gives, with the symmetric combination of the σ orbitals of the imidazole N1 atoms, an antibonding molecular orbital which is half occupied in Mn^{III} and empty in Mn^{IV}.

We can compare this structure to the numerous examples already reported containing the $[Mn_2O_2]^{3+}$ core.[16,27−29] The Mn−Mn axis is a C_2 axis as for $[Mn_2O_2(bispicen)_2]^{3+}$.[16] In other systems, the Mn−Mn axis is not an axis of symmetry, and the distances around each Mn atoms can be inequivalent as in $[Mn_2O_2(TPA)_2]^{3+}$ where the distances are $Mn^{III}-N_{ax}$ = 2.260 Å, 2.206 Å and $Mn^{IV}-N_{ax}$ = 2.012 Å, 2.014 Å.[30] The difference between the average Mn−N(axial ligand) distances around both Mn atoms reflects the asymmetry in electron distribution between the two Mn atoms. The Mn−N(axial ligand) distance difference is 0.204 Å in $[Mn_2O_2(bisimMe_2en)_2]^{3+}$ and ranges from 0.077 Å in $[Mn_2O_2(bispicen)_2]^{3+}$ to 0.29 Å in the cyclam analog.[29] With dimethyl-*N*,*N*′-bispicen, this difference is 0.16 Å.[31] The replacement of pyridine rings by imidazole rings seems to lead to a greater electron localization, although it is less than with cyclam. Following this criterion, $[Mn_2O_2(bispicen)_2]^{3+}$ would be the least localized of the series. This was already pointed out by Collins et al.[16]

In the structure, we note the presence of a water molecule at a distance of 2.714 Å from one oxo of the $[Mn_2O_2]^{3+}$ core.

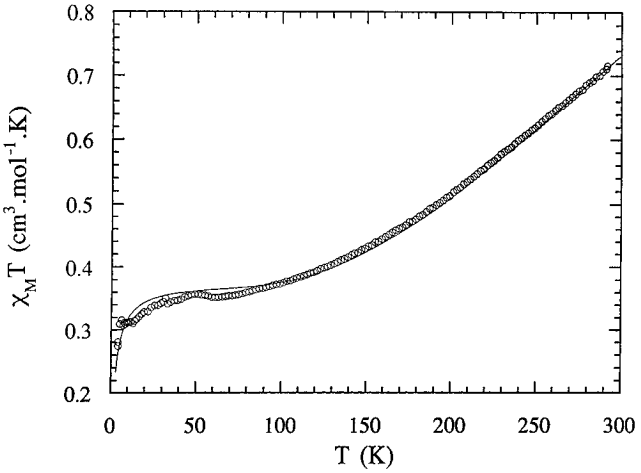

Figure 2. Product of the molar magnetic susceptibility by temperature per mole of $[Mn_2O_2(bisimMe_2en)_2]^{3+}$. The solid line was generated from the best fit parameters given in the text.

Magnetic Susceptibility Measurements. The molar magnetic susceptibility χ_M of a powder sample of $[Mn_2O_2(bisimMe_2en)_2](ClO_4)_3 \cdot H_2O$ was measured as a function of the temperature *T*. The results are shown in Figure 2 in the form of the $\chi_M T$ versus *T* plot. $\chi_M T$ decreases from 0.72 cm^3 mol^{-1} K at 291.6 K to a plateau at 0.35 cm^3 mol^{-1} K around 60 K. This is characteristic of an antiferromagnetic coupling between the electronic spins of the Mn^{IV} and Mn^{III} ions which produces a spin $S = {}^1/_2$ ground state. The decrease at low temperature was attributed to interactions between dinuclear units in the solid (this effect was modeled by introduction of the parameter θ in the expression below). The susceptibility was calculated as

$$\chi_M T = (N\beta^2 g^2 T/3k(T+\theta))(\sum S(S+1)(2S+1) \times \exp(JS(S+1)/2kT))/(\sum(2S+1)\exp(JS(S+1)/2kT))$$

The best fit was obtained by setting $g = 2$ for $J = -278$ cm^{-1} and $\theta = 1.82$ K. The *J* value is close to the $J = -280$ cm^{-1} reported for the bispicen analog.[32] The intermolecular interaction could be mediated by the water molecules noted in the crystallographic part.

EPR Spectra. The EPR spectrum of $[Mn_2O_2(bisimMe_2en)_2]^{3+}$ was recorded at 10 K in acetonitrile (Figure 3). This spectrum was simulated with the following parameters $|A_{1x,y}| = 160.10^{-4}$ cm^{-1}, $|A_{1z}| = 136.10^{-4}$ cm^{-1}, $|A_{2x,y}| = 72.10^{-4}$ cm^{-1}, $|A_{2z}| = 71.10^{-4}$ cm^{-1}, $g_{xy} = 1.997$, $g_z = 1.993$ with a line width equal to 20 G. This line width is larger than the one usually found in these systems: this could be related to the presence of more nitrogen atoms and the coupling of their nuclear spin with the electronic spin. As usual in these $Mn^{III}-Mn^{IV}$ complexes the anisotropy on Mn^{III} is such that $|A_{1x,y}| > |A_{1z}|$. This has been explained on the basis of the $d_\pi^3 d_z^{2\,1}$ ground state configuration for Mn^{III} in this type of complex:[33] these parameters would be intrinsically negative ($A_{1x,y} = -160.10^{-4}$ cm^{-1}, $A_{1z} = -136.10^{-4}$ cm^{-1}) and they would then obey the relation $A_{1z} > A_{1xy}$. Nevertheless, it should be noted that systematically this anisotropy (24×10^{-4} cm^{-1}, i.e. 12×10^{-4}

(27) Plaskin, P. M.; Stoufer, R. C.; Mathew, M.; Palenik, G. J. *J. Am. Chem. Soc*. **1972**, *94*, 2121−2122.

(28) Pal, S.; Gohdes, J. W.; Wilisch, W. C. A.; Armstrong, W. H. *Inorg. Chem*. **1992**, *31*, 713−716.

(29) Brewer, K. J.; Calvin, M.; Lumpkin, R. S.; Otvos, J. W.; Spreer, L. O. *Inorg. Chem*. **1989**, *28*, 4446−4451.

(30) Towle, D. K.; Botsford, C. A.; Hodgson, D. J. *Inorg. Chim. Acta* **1988**, *141*, 167−168.

(31) Verlhac, J. B.; Girerd, J.-J.; Guilhem, J. Unpublished results for the structure of $[Mn_2O_2(bispicMe_2en)_2](ClO_4)(BPh_4)_2 \cdot 2CH_3CN$. It is remarkable that the difference between axial Mn−N bonds is 0.186(7) Å in the recently published structure of $[Mn_2O_2(bispicMe_2en)_2](ClO_4)_3 \cdot H_2O$ (Glerup, J.; Goodson, P. A.; Hazell, A.; Hazell, R.; Hodgson, D. J.; McKenzie, C. J.; Michelsen, K.; Rychlewska, U.; Toftlund, H. *Inorg. Chem*. **1994**, *33*, 4105−4111). This suggests that the disymmetry in $Mn^{III}-Mn^{IV}$ systems could depend on lattice effects.

(32) Goodson, P. A.; Glerup, J. D.; Hodgson, D. J.; Michelsen, K.; Pedersen, E. *Inorg. Chem*. **1990**, *29*, 503−508.

(33) Zheng, M.; Khangulov, S. V.; Dismukes, G. C.; Barynin, V. V. *Inorg. Chem*. **1994**, *33*, 382−387.

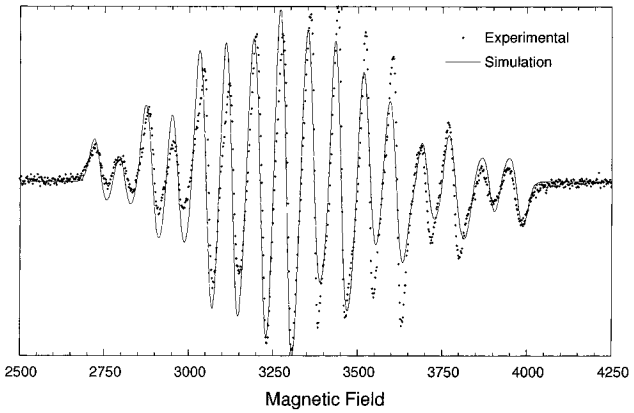

Figure 3. X-band cw-EPR spectrum of $[Mn_2O_2(bisimMe_2en)_2]^{3+}$ in acetonitrile (10 K, $\nu = 9.4086$ GHz). See text for the simulation.

cm^{-1} in the uncoupled scheme) is smaller than that measured in Mn^{III} monomers (30×10^{-4} cm^{-1}).[34] The origin of this effect is still unclear.

EPR and ESEEM spectra were recorded in aqueous borate buffer. The field-swept echo of the $[Mn_2O_2(bisimMe_2en)_2]^{3+}$ complex in borate buffer at pH = 10 is represented in Figure 4 (panel A). The derivative is represented in Figure 4B. It is very similar to the CW-EPR spectrum in the same conditions (Figure 4C).

The 2D ESEEM frequency spectrum has been recorded at 3480 G (Figure 5). For clarity, the τ values increase from the back to the front of the graph. The inset shows the ESEEM in the time domain for the minimum τ and T values used i.e. 120 ns and 24 ns, respectively.

The complexity of the ESEEM spectrum presumably reflects hyperfine interactions from the 8 to 12 ^{14}N which could, in principle, be coupled to the Mn nuclei. Frequencies were observed at 1.19, 2.23, 2.47, 2.78, 3.63, and 5.1 MHz for 3480 G. In order to properly attribute the ESEEM frequencies, specific $^{14}N/^{15}N$ exchange at each nitrogen position is required. This was not done in the present work. Tan et al.[35] observed, by ENDOR, nitrogen resonances in cyclam and TPA $Mn^{III}Mn^{IV}$ complexes. They attributed these resonances to the nitrogen atoms linked to the Mn^{III}. The same type of analysis was proposed in an ENDOR study of the bpy $Mn^{III}Mn^{IV}$ complex.[36] Adopting their view and taking $e^2Qq = 3$ MHz, $\nu(^{14}N, 3480\ G) = 1.07$ MHz, one can consider that the resonances at 2.78 and 5.1 MHz are the two components of one doublet coming from nitrogen atoms strongly coupled ($A = 12.4$ MHz) to the electronic spin. These would be the nitrogens linked to the Mn^{III} ion. This large coupling value is reasonable when one compares the $N-Mn^{III}$ distances: cyclam, 2.35 Å, 9.23 MHz; TPA, 2.23 Å, 11.2 MHz; $bisimMe_2en$, 2.208 Å, 12.4 MHz. This correlation has already been made by Tan et al.[35] If these attributions are correct, the other resonances could originate from nitrogen atoms that are more weakly coupled. A completely different interpretation of this ESEEM spectrum would be to suppose that the nitrogen atoms directly linked to Mn^{III} are too strongly coupled to be observed in ESEEM as happens in imidazole−Cu^{II} systems.[37] The resonances would then come from the remote nitrogen of the imidazoles and the nitrogens of the ethylenediamine unit. A surprising result in Figure 5, is the absence of the 15 MHz feature which corresponds to the free

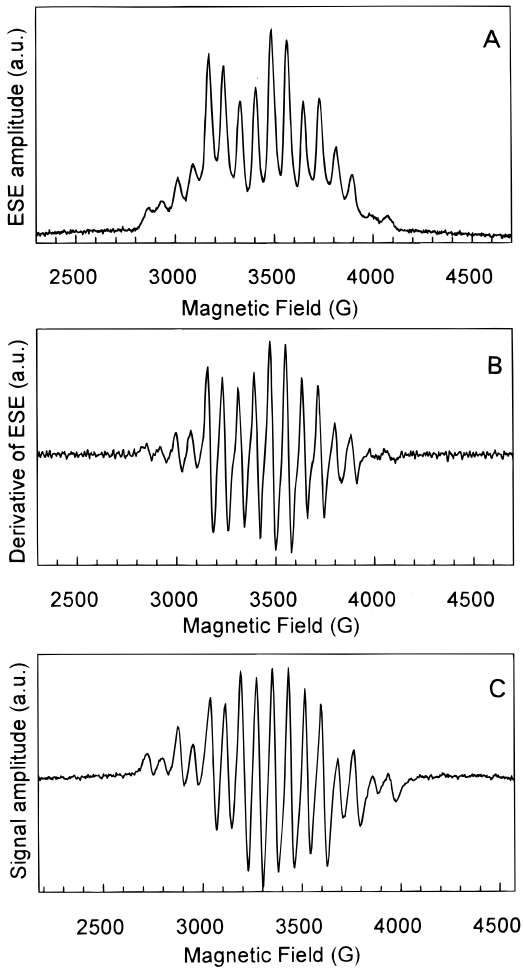

Figure 4. Panel A: Field-swept echo of $[Mn_2O_2(bisimMe_2en)_2]^{3+}$ in borate buffer at pH 10. Instrument settings: the amplitude of the echo results from a two-pulse sequence ($\pi/2 = 8$ ns, $\tau = 376$ ns, $\pi = 16$ ns); temperature, 4−5 K; microwave frequency, 9.7 GHz. Panel B: Derivative spectrum of the field-swept echo shown in panel A. Panel C: cw-EPR spectrum of $[Mn_2O_2(bisimMe_2en)_2]^{3+}$ in borate buffer at pH 10. Instrument settings: temperature, 4 K; modulation amplitude, 10 G; microwave power, 20 mW; microwave frequency, 9.4 GHz; modulation frequency, 100 KHz.

proton frequency. This indicates that even in aqueous media the $Mn^{III}-Mn^{IV}$ core is isolated from the solvent. By changing the solvent from H_2O to D_2O, an important 2.4 MHz peak appeared (not shown). This has to be compared to the Larmor frequency $\nu(^2H, 3480\ G) = 2.27$ MHz. This could correspond to the hydrogen atoms of the amino nitrogens of the imidazole rings. This method of detecting hydrogen resonances in ESEEM has been already used in ref 38.

UV-vis. The spectrum of the [III,IV] species in acetonitrile has been recorded. Maxima are measured at 644 nm (304 M^{-1} cm^{-1}), 536 nm (428 M^{-1} cm^{-1}), and 419 nm (950 M^{-1} cm^{-1}). From a recent detailed study[39] one can attribute these bands as follows: the 644 nm band includes Mn^{IV} oxo LMCT bands; the 536 and 419 nm bands are due to Mn^{IV} d−d transitions. They are likely to be two of the components of the $^4A_{2g} \rightarrow {}^4T_{2g}$ transition. Following, Gamelin et al.,[39] the Mn^{III} d−d transitions lead to weaker bands which are hidden in this type of spectrum.

II. Redox Properties of the $[Mn_2O_2(bisimMe_2en)_2]^{3+}$ Species. Electrochemistry. Cyclic voltammetry of $[Mn_2O_2$-

(34) Gerritsen, H. J.; Sabisky, E. S. *Phys. Rev.* **1963**, *132*, 1507−1512.
(35) Tan, X.; Gultneh, Y.; Sarneski, J. E.; Scholes, C. P. *J. Am. Chem. Soc.* **1991**, *113*, 7853−7858.
(36) Khangulov, S.; Sivaraja, M.; Barynin, V. V.; Dismukes, G. C. *Biochemistry* **1993**, *32*, 4912−4924.
(37) Mims, W. B.; Peisach, J. *J. Chem. Phys.* **1978**, *69*, 4921−4930.
(38) Lee, H. C.; Wittenberg, J. B.; Peisach, J. *Biochemistry* **1993**, *32*, 500−11506.
(39) Gamelin, D. R.; Kirk, M. L.; Stemmler, T. L.; Pal, S.; Armstrong, W. H.; Penner-Hahn, J. E.; Solomon, E. I. *J. Am. Chem. Soc.* **1994**, *116*, 2392−2399.

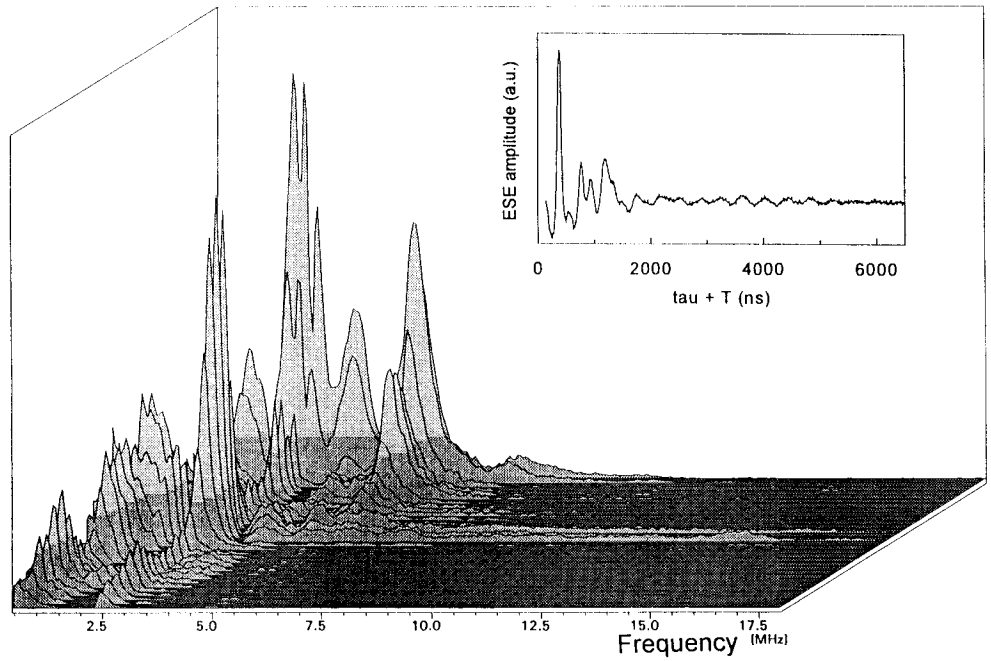

Figure 5. 2D frequency spectrum recorded at 3480 G (position 1 in Figure 10, but with the same concentration that in Figure 4) in the $[Mn_2O_2(bisimMe_2en)_2]^{3+}$ signal. For reason of clarity the τ value was incremented from the back to the front of the graph. The inset shows the ESEEM in the time domain for the minimum τ and T values used, i.e. 120 ns and 24 ns, respectively.

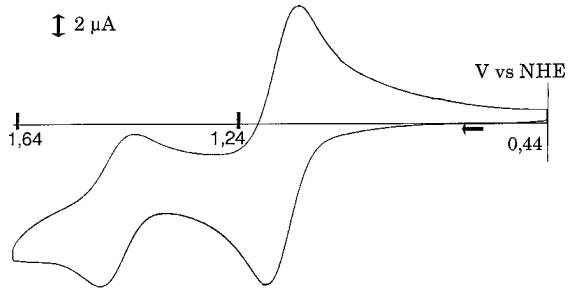

Figure 6. Cyclic voltammetry of $[Mn_2O_2(bisimMe_2en)_2]^{3+}$ in acetonitrile at room temperature. TBAP was used as electrolyte.

$(bisimMe_2en)_2]^{3+}$ obtained in acetonitrile is shown in Figure 6. Two anodic reversible waves are observed at $E_{1/2} = 1.04$ and 1.40 V. The ΔE_p values are, respectively, 65 and 76 mV. The intensity of the first wave is twice that of the second. Increasing the potential sweep rate for each wave indicates that both are controlled by diffusion process in the range 50 mV s^{-1} to 300 mV s^{-1}. Use of higher scan rates did not allow to detect any change in the CV. The presence of two oxidation waves is in strong contrast with the observation of only one oxidation wave ([III,IV] → [IV,IV]) for $[Mn_2O_2(bispicen)_2]^{3+}$ at 0.99 V[16] and for $[Mn_2O_2(bispicMe_2en)_2]^{3+}$ at 1.39 V.

Preparative scale electrolysis was run at $E = 1.19$ V and indicated that one electron per two Mn is involved. After total electrolysis of the solution at $E = 1.19$ V, the potential was set at 1.64 V. Total electrolysis at this potential involves approximately 0.4 electron per two Mn.

EPR Spectroelectrochemistry. In order to characterize the different species formed during the redox processes, EPR spectra were recorded on electrochemically prepared solutions. Two sets of experiments were carried out. In the first type of experiments, the oxidized species was generated in an electrochemical cell (using a Pt grid) which was mounted in the EPR cavity. In the second type of experiment, products of the preparative electrolysis in an opaque cell, were transferred into an EPR tube.

Figure 7A shows the evolution of the room temperature EPR spectrum during electrolysis at $E = +1.24$ V. The starting spectrum displays the 16 lines characteristic of the [III,IV] species although it is less well resolved than in frozen solution. After 1 h of electrolysis the signal disappeared. Changing the potential to $E = 1.74$ V allowed the observation of an intense 6-line spectrum after a few minutes. This spectrum is characterized by an hyperfine coupling $a = 88.10^{-4}$ cm^{-1}, in the range of values observed for Mn^{II}.[40] This 6-line spectrum disappears when resetting the potential of the working electrode at 0.64 V and the 16-line spectrum is observed, indicating the presence of the [III,IV] species in solution. The complete oxidation/reduction sequence was then reproduced on the same sample, starting with the [III,IV] species, oxidizing it at 1.74 V (6-line spectrum), and rereducing it at 0.64 V (16-line spectrum). On the basis of integration of the EPR spectra, 75% of the starting species was recovered at the end of each cycle. The reversibility of the overall process is remarkable.

Figure 7B represents the spectrum of $[Mn_2O_2(bisimMe_2en)_2]^{3+}$ at room temperature in CH_3CN before and after oxidation at 1.24 V using the bulk electrolysis cell. After the oxidation, the 16-line spectrum has practically disappeared. The disappearance of the EPR signal after oxidation by one electron of the [III,IV] pair is expected and agrees with a [IV,IV] dimer formulation.

UV-vis Spectroelectrochemistry. Oxidation at 1.24 V has been followed by UV-vis. Under 572 nm, the absorption of the oxidized form is stronger than that of the [III,IV] complex. The same observation has been made by Brewer et al.[29] in spectroelectrochemical oxidation of $[Mn_2O_2(14\text{-ane } N_4)_2]^{3+}$ to the corresponding [IV,IV] form. Above 572 nm, the absorption of the oxidized form is weaker than that of the [III,IV] form. A complementary experiment has been done by UV-vis spectroelectrochemistry (Figure 8) on a solution of $[Mn_2O_2(bisimMe_2en)_2]^{3+}$ using a 0.5 mm cell and a diode array spectrophotometer. At high energy, an important increase of the molar absorption is observed, which is likely related to $O \rightarrow Mn^{IV}$ LMCT bands. These observations are in agreement with the formation of the [IV,IV] dimer at this potential.

(40) Whittaker, J. W.; Whittaker, M. M. *J. Am. Chem. Soc.* **1991**, *113*, 5528−5540 and references therein.

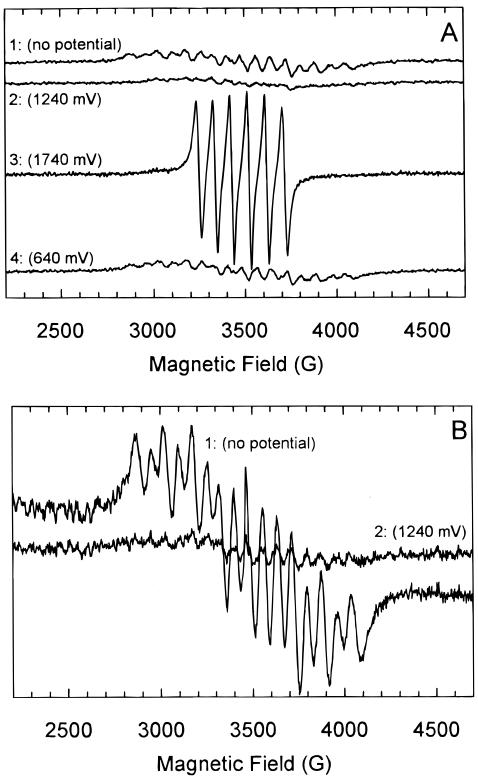

Figure 7. EPR spectroelectrochemistry at room temperature in CH_3CN. (A) One complete cycle using a spectroelectrochemical EPR cell. (B) EPR spectra before and after oxidation in a dark bulk electrolysis cell: (1) accumulated signal for $[Mn_2O_2(bisimMe_2en)_2]^{3+}$; (2) spectrum of the oxidized species at 1.24 V. Instrument settings: modulation amplitude, 20 G; microwave power, 20 mW; microwave frequency, 9.4 GHz; modulation frequency, 100 KHz.

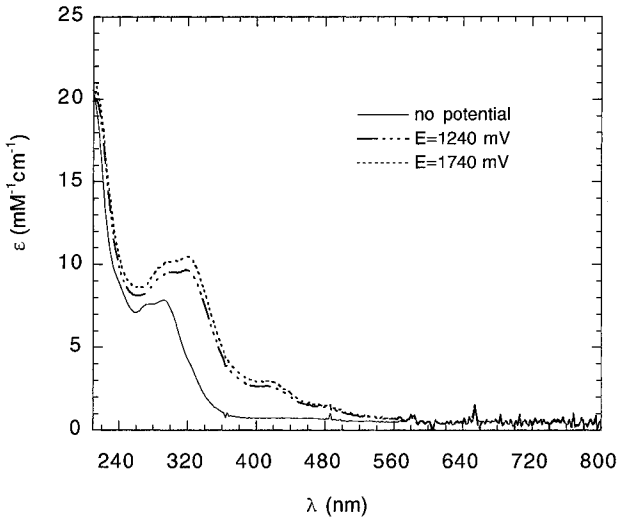

Figure 8. UV-vis spectroelectrochemistry of $[Mn_2O_2(bisimMe_2en)_2]^{3+}$ in acetonitrile at room temperature.

Oxidation at 1.74 V gives a spectrum with slightly higher optical density than at 1.24 V, but the spectra are very similar. The corresponding species is sensitive to light since with a normal spectrophotometer, we observed a rapid diminution of the OD at 1.74 V.

The observation of two oxidation waves is difficult to understand. Our preferred hypothesis is that a slow (relatively to the scan-rate used in CV) equilibrium exists between two forms of the [III,IV] dimer. By electrolysis at $E = 1.24$ V, this equilibrium could be displaced to give a [IV,IV] dimer with 100 % yield.[41] The following equilibria would exist

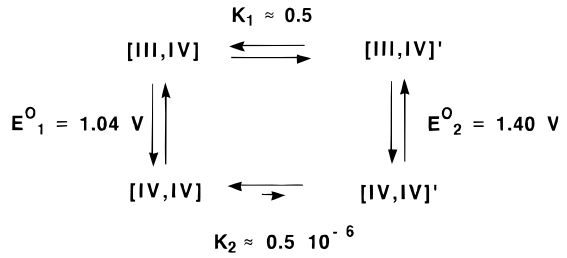

The energetic differences between the two forms would be small for the [III,IV] state but much larger for the [IV,IV] state (≈0.36 eV).

What can be the origin of such an equilibrium? It could be related to the existence of two structural isomers: one acceptable hypothesis is that one would have a cis α local geometry around each Mn ion (as characterized in solid state), the other a cis β local geometry. Another possibility could be that only one metal center is concerned by this change in configuration (isomers αα and αβ).[17] If our interpretation is correct, ESEEM spectroscopy (see above) and paramagnetic NMR would give informations on both isomers and could allow a study of this equilibrium. It can be difficult to detect these isomers by cw-EPR or UV-vis spectroscopy.

We have not yet fully understood the observation of the 6-line spectrum at $E = 1.74$ V. We consider presently that it is not related to the second wave observed in CV but is due to a partial oxidation of the [IV,IV] species accumulated at 1.24 V. A possibility is that at such a high potential, Mn^V could be attained but the ligand would then be oxidized, giving back Mn^{II}.

III. Low Temperature UV Illumination. To generate an organic radical in the [III,IV] complex, the sample was UV-irradiated at 77 K. Figure 9 (spectrum a) shows the spectrum recorded by cw-EPR prior to UV illumination using a diluted sample; it is the characteristic 16-line spectrum from the [III,IV] species. After UV irradiation at 77 K the 16-hyperfine lines disappeared and a new signal appeared (spectrum b). This new signal was centered at $g = 2.0049$ and had a width of about 50 gauss. In addition, a broad unresolved slightly asymmetric signal was present between 2700 G and 4000 G. The narrow radical does not appear to be split like that reported in PSII in Ca^{2+}-depleted enzyme. However, it is of note that in SO_4^{2-}-treated enzyme, the S_3 signal is unresolved[11] like that observed in the model complex.

Figure 9 inset A shows the amplitude of the multiline signal versus the amplitude of the UV-induced signal. The points were recorded by varying the time of UV-illumination. It shows clearly that the appearance of the narrow signal at $g = 2.0049$ followed exactly the disappearance of the multiline signal. Therefore, this experiment shows that no intermediate species could be detected. The effects are similar to those seen in PS II, in which an inverse relationship between the presence of an organic radical and the Mn multiline signal was observed. The interpretation of the disappearance of the Mn signal being due to a magnetic interaction with the organic radical rather than to oxidation of the Mn cluster is consistent with the results seen in Figure 9. Unlike the biological system, however, in which the radical is formed with a high quantum yield due to the high

(41) Two informations which will be developed in a future paper are relevant here. When CV is done on a solution electrolyzed at 1.19 V, the wave at 1.04 V increases spectacularly. We prepared a new ligand *N*,*N*′-dimethyl-*N*,*N*′-bis[(1-methylimidazol-2-yl)methyl]ethane-1,2-diamine and the corresponding [III,IV] complex. This complex exhibits again two waves in CV around the same potentials but with a different intensity ratio. We explained this behavior with a different K_1 value.

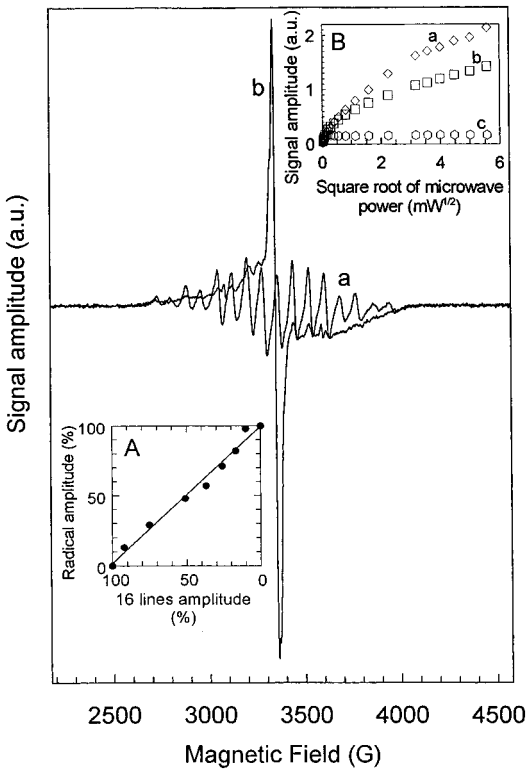

Figure 9. cw-EPR spectra of $[Mn_2O_2(bisimMe_2en)_2]^{3+}$ in borate buffer at pH 10 prior to UV irradiation (spectrum a) and after UV irradiation (spectrum b). Instrument settings: temperature, 4 K; modulation amplitude, 10 G; microwave power, 20 mW; microwave frequency, 9.4 GHz; modulation frequency, 100 KHz. Inset A: Amplitude of the radical signal versus the amplitude of the 16-line signal. The different points were obtained by varying the time of UV irradiation. The straight line through the points has been obtained by a linear fit procedure. Instrument settings as in Figure 4 (panel C). Inset B: Microwave power saturation of the $Mn^{III}-Mn^{IV}$ signal (curve a), of the radical induced by UV irradiation of $[Mn_2O_2(bisimMe_2en)_2]^{3+}$ in borate buffer at pH 10 (curve b) and of the 4-methylimidazole radical alone induced by UV irradiation (curve c). Instrument settings as in Figure 4 (panel C). The signals are normalized to the same amplitude at low microwave power, i.e. in nonsaturating conditions.

efficiency of the reaction center, for the UV-generated radical, we cannot rule out the occurrence of an intermediate step of Mn oxidation followed by radical formation if the formation of the former was the rate-limiting step in the two-step reaction. Formation of a ligand radical by irradiation at 254 nm of $Mn^{II}{}_2$-$Mn^{III}{}_2$ tetranuclear system has already been observed.[42]

Figure 9 inset B shows the microwave power saturation of the $Mn^{III}-Mn^{IV}$ signal (curve a) of the radical induced by UV irradiation of $[Mn_2O_2(bisimMe_2en)_2]^{3+}$ (curve b) and of 4-methylimidazole radical alone (curve c). The amplitudes of the three signals are normalized at low microwave power i.e. in nonsaturating conditions. The radical induced in $[Mn_2O_2(bisimMe_2en)_2]^{3+}$ shows saturation properties very similar to the Mn dimer signal, being more difficult to saturate than the 4-methylimidazole alone. This indicates that the radical induced in $[Mn_2O_2(bisimMe_2en)_2]^{3+}$ is close to the Mn. The same experiment done with sample at higher or lower concentrations resulted in similar results. This indicates that the radical induced in the sample is part of $[Mn_2O_2(bisimMe_2en)_2]^{3+}$. In PS-II, the S_3 radical signal shows relaxation characteristics like those of the Mn multiline signal.[43]

In Figure 10, the field-swept echo spectra of the [III,IV] complex are shown before and after UV illumination. The loss

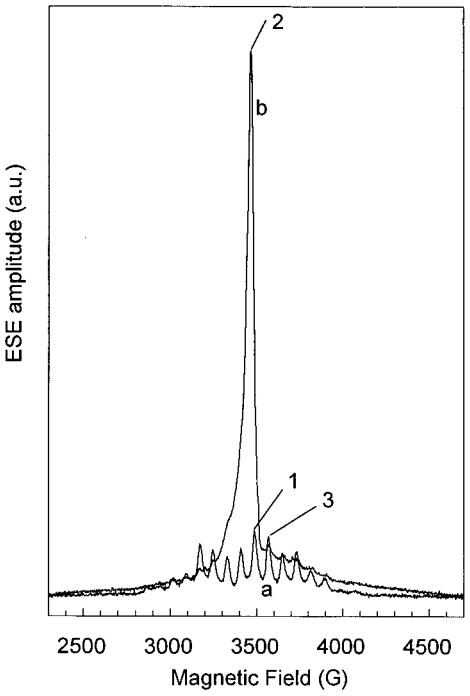

Figure 10. Field-swept echo of $[Mn_2O_2(bisimMe_2en)_2]^{3+}$ in borate buffer at pH 10 prior to UV irradiation (spectrum a) and after UV irradiation (spectrum b). No normalization procedure was used to plot the field-swept spectra. Instrument settings: the amplitude of the echo results from a two-pulse sequence ($\pi/2 = 8$ ns, $\tau = 376$ ns, $\pi = 16$ ns); temperature, 4−5 K; microwave frequency, 9.7 GHz.

of the characteristic hyperfine lines of the [III,IV] complex and the appearance of a narrow radical-like signal is seen just as in the CW experiments shown in Figure 9. In the field-swept echo spectrum, a very broad signal is detected in the sample after illumination. Integration of spectra a and b indicates that UV irradiation induced an approximate doubling of the number of spins. A more accurate measurement was precluded by the fact that dilute samples had to be used for the photooxidation experiment. Further illumination (up to double the illumination time used in the experiment shown) resulted in no further changes to the EPR spectra (not shown).

In PSII, a broad featureless field-swept echo signal was observed after formation of the S_3 radical signal which is similar to that seen in Figure 10b. This signal was attributed to the Mn cluster in the spin $^1/_2$ state, and the absence of the hyperfine lines was explained by the presence of a magnetic interaction with the radical. The broad signal seen in Figure 10b could have an analogous origin.

A first interpretation of the spectrum of the radical containing species would rely only on the theory of exchange interaction between 2 spins $S = {}^1/_2$ with Lande factors g_1 and g_2. In that case, four resonances can be observed, two outer lines and two inner lines, the inner lines being close to g_1 and g_2 and the outer lines being on each side of the central lines; when $|J|$ increases, the outer lines move away from the central lines which themselves move toward a common resonance at $(g_1 + g_2)/2$.[44,45] Such spectra have been observed at room temperature in fluid solution for spin-labeled ligands coordinated to Cu^{II}.[46]

(42) Thorp, H. H.; Sarneski, J. E.; Kulawiec, R. J.; Brudvig, G. W.; Crabtree, R. H.; Papaefthymiou, G. C. *Inorg. Chem.* **1991**, *30*, 1153−1155.

(43) Boussac, A.; Zimmermann, J.-L.; Rutherford, A. W. *Proceedings of the 8th International Congress on Photosynthesis*, Stockholm, 1989; Kluwer: Dordrecht, The Netherlands; Vol. I, pp 713−716.

(44) Abragam, A.; Bleaney, B. *Electron Paramagnetic Resonance of Transition Ions*; Oxford University Press: New York, 1970.

(45) Eaton, S. S.; DuBois, D. L.; Eaton, G. R. *J. Magn. Reson.* **1978**, *32*, 251−263.

(46) Boymel, P. M.; Braden, G. A.; Eaton, G. R.; Eaton, S. S. *Inorg. Chem.* **1980**, *19*, 735−739.

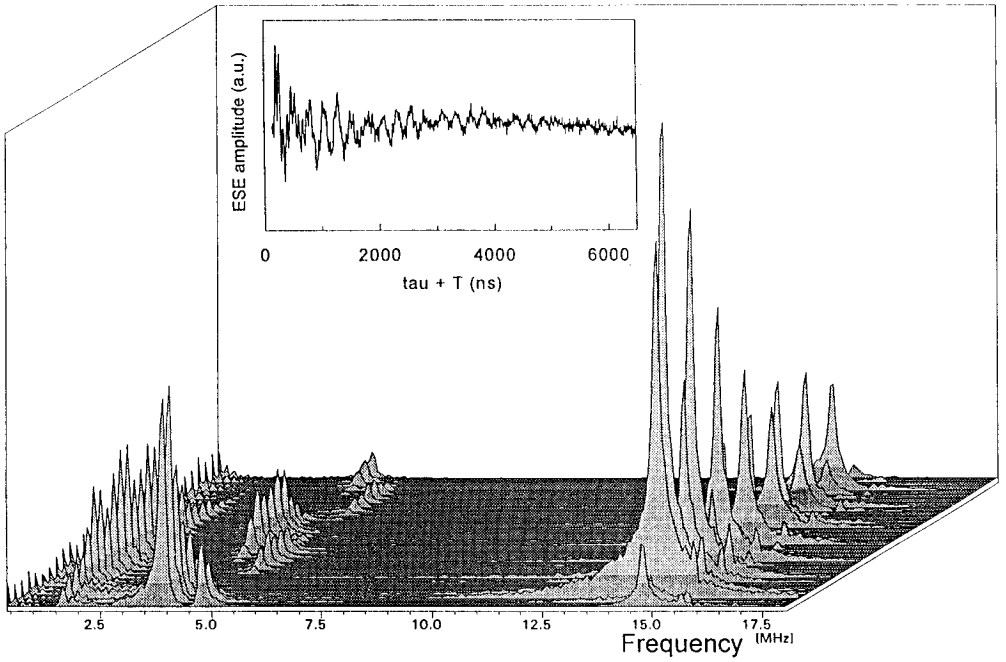

Figure 11. 2D frequency spectrum recorded in the radical induced by UV irradiation of $[Mn_2O_2(bisimMe_2en)_2]^{3+}$ (position 2 in Figure 10).

In the case of interest here, the g factors of the [III,IV] pair (see above) and the neutral 4-methylimidazole radical ($g = 2.0047$)[47] are such that $(g_1 - g_2)\beta H = 15 \times 10^{-4}$ cm^{-1} at 3300 G. With such a small value for the difference in Zeeman energies, one understands that small variations in J will be critical on the appearance of the signal. This could explain why the width of the radical S_3 signal is so dependent on biochemical treatments, being for instance much narrower in Cl^--depleted enzyme than in the Ca^{2+}-depleted enzyme.[48] Here $|J|$ must be of the order of the width of the radical signal (50 G = 50 × 10^{-4} cm^{-1}). This explains also why the hyperfine lines are no longer resolved in the manganese signal. This has also been observed in a series of spin-labeled ligands coordinated to Mn^{II} studied by More et al.[49] The J coupling is larger in the Ca^{2+}-depleted S_3 state than in the irradiated [III,IV].

Interpretation of frozen solution spectra certainly need dipolar effects to be added to exchange interaction.[50−52]

After UV irradiation, ESEEM was done on the signal at 3460 gauss (position 2 in Figure 10). The 2D frequency spectrum is shown in Figure 11. The inset shows the ESEEM in the time domain for the minimum τ and T values used, i.e. 120 and 24 ns, respectively. The 15 MHz feature corresponding to the free proton frequency is detected. This seems reasonable since the radical spin is at the periphery of the complex. Moreover, three peaks can be resolved at 1.6, 3.7, and 4.7 MHz.

As the radical in $[Mn_2O_2(bisimMe_2en)_2]^{3+}$ can be formed with a high yield only in diluted samples, the frequency spectrum obtained after UV irradiation in the Mn signal at a field position outside the radical signal (i.e. at 3560 gauss, position 3 in Figure 10) was only performed in 1D with a τ value of 120 ns. Figure 12 panel A shows the ESEEM in the time domain, and panel B

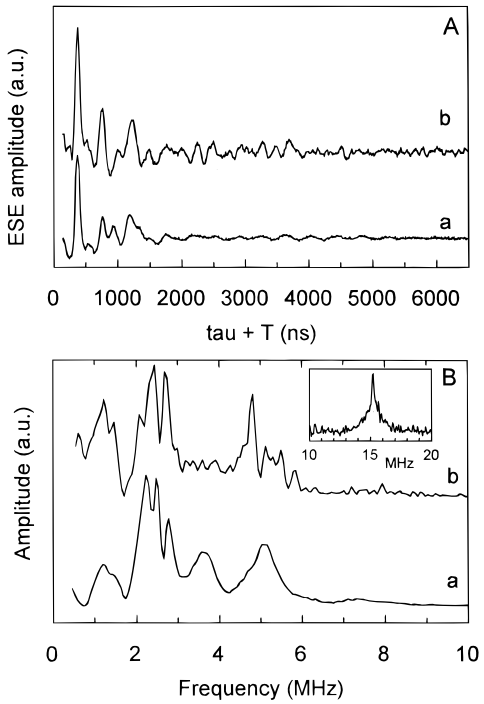

Figure 12. ESEEM in the time domain (upper panel) and in the frequency domain (lower panel) recorded at 3560 G (position 3 in Figure 10) in the $[Mn_2O_2(bisimMe_2en)_2]^{3+}$ signal prior to illumination (curves a) or after formation of the radical (curves b). The τ and T values used were 120 and 24 ns, respectively. The inset shows the 15 MHz region recorded with τ and T values of 184 and 24 ns, respectively, after the UV illumination procedure.

in the frequency domain. Spectra a were recorded prior to UV irradiation (with a concentrated sample), and spectra b were recorded after radical formation (on a diluted sample). Considering the low signal to noise ratio in the sample used for the UV illumination the couplings observed in the Mn signal seems not significantly modified by the formation of the radical. A major difference is nevertheless observed since for a τ value which did not suppress the free proton frequency (i.e. 184 ns), a peak at 15 MHz could be observed after UV illumination (inset

(47) Berthomieu, C.; Boussac, A. *Biospectroscopy* **1995**, *1*, 187−206.
(48) Boussac, A.; Sétif, P.; Rutherford, A. W. *Biochemistry* **1992**, *31*, 1224−1234.
(49) More, J. K.; More, K. M.; Eaton, G. R.; Eaton, S. S. *J. Am. Chem. Soc.* **1984**, *106*, 5395−5402.
(50) Eaton, S. S.; More, K. M.; Sawant, B. M.; Boymel, P. M.; Eaton, G. R. *J. Magn. Reson.* **1983**, *52*, 435−449.
(51) Eaton, S. S.; More, K. M.; Sawant, B. M.; Eaton, G. R. *J. Am. Chem. Soc.* **1983**, *105*, 6560−6567.
(52) Bertrand, P.; More, C.; Guigliarelli, B.; Fournel, A.; Bennett, B.; Howes, B. *J. Am. Chem. Soc.* **1994**, *116*, 3078−3086.

of panel B). This could be due to the fact that now the metal core senses the solvent protons via the magnetic interaction with the radical.

Finally it is not easy to decide if the imidazole radical stays as a ligand or if it separates from the metal core. On one hand the weakness of the magnetic interaction would suggest that the radical is no longer a ligand; on the other hand, it is known that magnetic interaction are very sensitive to orbital overlaps; it may happen that two spins are close and that for symmetry reasons their interaction is weak. The reduced spin density on the nitrogen atoms of the imidazole radical can also explain the weakness of the magnetic interaction. The observation of a very weak 15 MHz ESEEM resonance in Figure 12b, may indicate that the metal core is not exposed to the solvent and that the ligand is still linked. Lastly, the illumination is made at 77 K, and it seems difficult to have a substitution reaction at this temperature.

Conclusion

The first complex with an imidazole ligand linked to a $Mn^{III}-Mn^{IV}$ core has been obtained and characterized. The ESEEM spectrum has been reported. Frequencies related to nitrogens and hydrogens (using D_2O) were observed. In contrast to analogous complexes described with ligands of the bispicen family, in cyclic voltammetry, two oxidation waves were observed. The two waves do not have the same intensity. By EPR spectroelectrochemistry at room temperature, the disparition, upon oxidation at 1.24 V, of the 16-line spectrum characteristic of the [III,IV] species, was followed. UV-vis spectroelectrochemistry agrees with the formation of the [IV,IV] species. The presence of two waves in CV, can be interpreted as due to a slow equilibrium between two forms of the [III,IV] mixed-valent dimer. At higher potential (1.74 V), a 6-line EPR signal was observed which could be due to formation of Mn^{II} after oxidation of the ligand by Mn^{V}. UV irradiation of the $[Mn_2O_2(bisimMe_2en)_2]^{3+}$ system at low temperature in a borate buffer at pH = 10, gives a radical species in magnetic interaction with the $Mn^{III}-Mn^{IV}$ cluster. ESEEM spectra were obtained at magnetic field values characteristic of the radical or the [III,IV] complex. Some arguments have been given in favor of the maintenance of the structure after irradiation. Although the spectroscopic data obtained for the state generated by UV treatment of the [III,IV] complex are not identical to those obtained in S_3 state in the inhibited enzyme, they are sufficiently close to warrant future detailed comparative studies with this complex and related model systems we have prepared. Indeed, the similarities in the spectroscopic data are such that the possibility that the S_3 radical is a direct ligand to Mn cluster should be reconsidered.

Acknowledgment. We are grateful to Dr Sun Un for helpful discussions.

Supporting Information Available: Tables of positional and thermal parameters for all atoms, of interatomic distances and angles, anisotropic temperature factors (4 pages); observed and calculated structure factors (4 pages). This material is contained in many libraries on microfiche, immediately follows this article in the microfilm version of the journal, can be ordered from ACS, and can be downloaded from the Internet; see any current masthead page for ordering information and Internet access instructions.

JA9436411